ACS APPLIED MATERIALS & INTERFACES

Research Article

www.acsami.org

Green-Sensitive Organic Photodetectors with High Sensitivity and Spectral Selectivity Using Subphthalocyanine Derivatives

Kwang-Hee Lee,[†,‡] Dong-Seok Leem,[†] Jeffrey S. Castrucci,[§] Kyung-Bae Park,[†] Xavier Bulliard,[†] Kyu-Sik Kim,[†] Yong Wan Jin,*[,†] Sangyoon Lee,[†] Timothy P. Bender,[§] and Soo Young Park*[,‡]

[†]Emerging Materials Center, Samsung Advanced Institute of Technology, Samsung Electronics Co., Yongin 446-712, Republic of Korea

[‡]Center for Supramolecular Optoelectronic Materials, Department of Materials Science and Engineering, Seoul National University, 1 Gwanak-ro, Gwanak-gu, Seoul 151-744, Republic of Korea

[§]Department of Chemical Engineering and Applied Chemistry, University of Toronto, 200 College Street, Toronto, Ontario M5S 3E5, Canada

Supporting Information

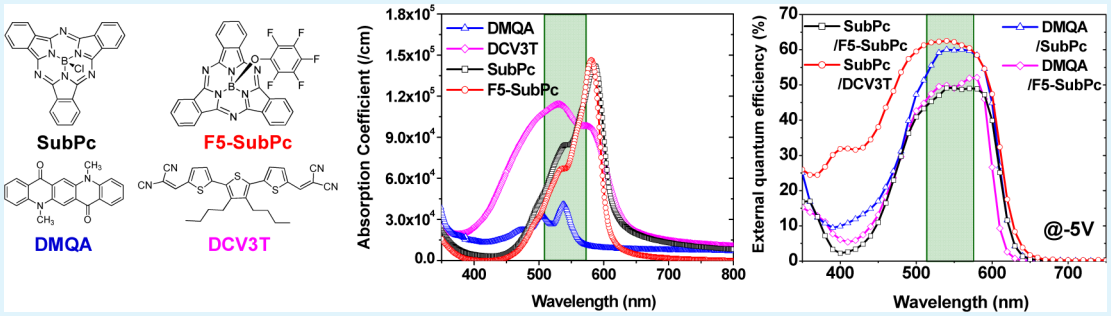

ABSTRACT: Green-sensitive organic photodetectors (OPDs) with high sensitivity and spectral selectivity using boron subphthalocyanine chloride (SubPc) derivatives are reported. The OPDs composed of SubPc and dicyanovinyl terthiophene derivative (DCV3T) demonstrated the highest green-sensitivity with maximum external quantum efficiency (EQE) of 62.6 % at an applied voltage of −5 V, but wide full-width-at-half-maximum (FWHM) of 211 nm. The optimized performance considering spectral selectivity was achieved from the composition of *N*,*N*-dimethyl quinacridone (DMQA) and SubPc showing the high specific detectivity (D^*) of 2.34×10^{12} cm $Hz^{1/2}/W$, the EQE value of 60.1% at −5 V, and narrow FWHM of 131 nm. In spite of the sharp absorption property of SubPc with the maximum wavelength (λ_{max}) at 586 nm, the EQE spectrum showed favorable green-sensitivity characterized by smooth waveform with λ_{max} at 560 nm, which is induced from the high reflectance of SubPc centered at 605 nm. The photoresponsivity of the OPD devices was found to be consistent with their absorptance. Optimized DMQA/SubPc device showed the lowest value of blue crosstalk (0.42) and moderate red crosstalk (0.37), suggesting its promising application as a green-sensitive OPD.

KEYWORDS: *organic photodetector, subphthalocyanine, green-sensitivity, selectivity, crosstalk, image sensor*

INTRODUCTION

The increasing interest for artificial vision for future applications such as artificial intelligence has boosted up the technology development of artificial eyes, image scanners, and image sensors.[1−4] Most of all, the development of image sensors based on complementary metal oxide semiconductor (CMOS) circuits has been considerably accelerated in response to the demands for mobile phone cameras with higher resolution and lower noise level.[5] The Si photodiode (Si PD) in conventional CMOS image sensor (CIS), with the combined advantages of high photoelectric conversion efficiency with low dark current, has been dominating the market and the imaging technology development.[6] However, the inherent properties of Si PD such as nonselective color sensitivity in the visible region and low absorption coefficient are not optimal, implying the addition of a color separation system resulting in thick photodiode devices. This also induces undesirable pixel-to-pixel crosstalk in the photodiode that generates harmful noise against the color correction in CIS device.[7]

Crosstalk in an image sensor array results from three different contributions: spectral crosstalk due to imperfect color separation, optical spatial crosstalk induced by the transmission of unabsorbed light to an adjacent pixel, and electrical crosstalk by movement of the photogenerated carriers to the neighboring pixel.[8] Alternative candidates for the replacement of Si PD have been investigated for their high sensitivity with high coefficient

Received: September 22, 2013
Accepted: November 25, 2013
Published: November 25, 2013

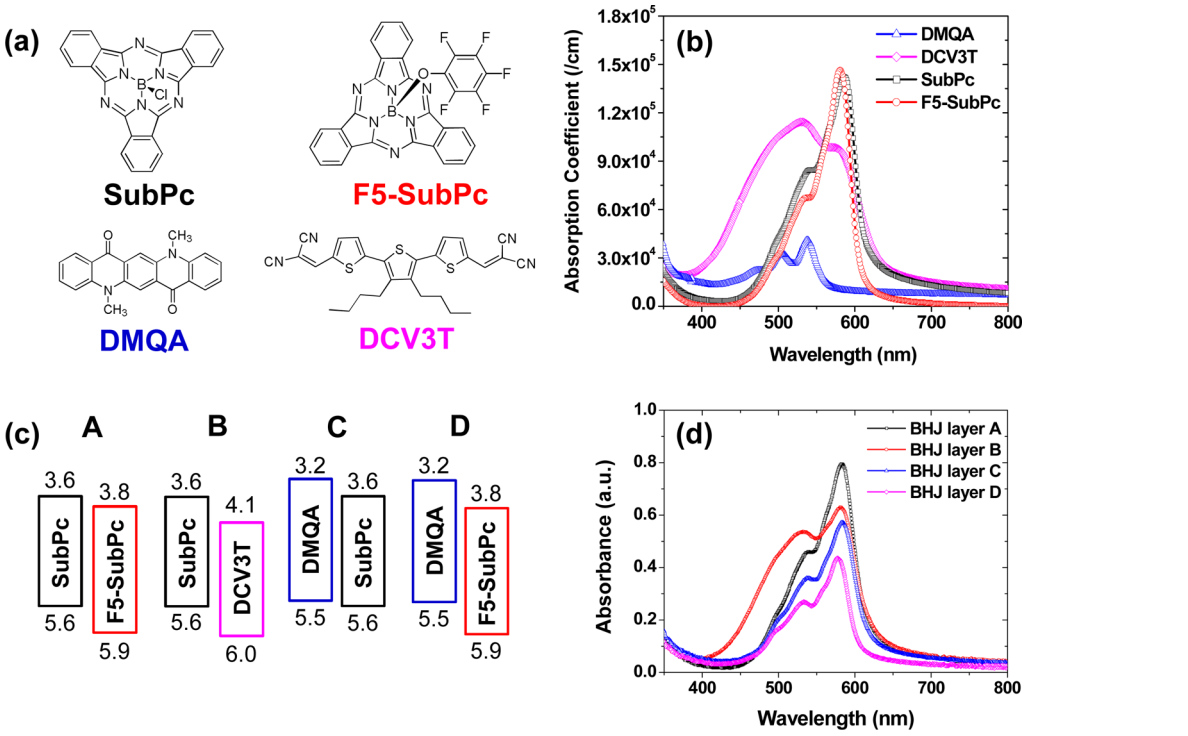

Figure 1. (a) Molecular structures of boron-subphthalocyanine chloride (SubPc), pentafluoro-phenoxy-substituted SubPc (F5-SubPc), *N*,*N*-dimethyl quinacridone (DMQA), and dibutyl-substituted dicyanovinyl terthiophene (DCV3T). (b) Absorption coefficients of the four active materials measured by UV−vis spectroscopy. (c) Energy level diagrams of donor/acceptor compositions for the four basic OPD devices. (d) Absorbance spectra of the four BHJ layers.

of absorption in order to reduce the optical and electrical crosstalk, simultaneously. Among inorganic semiconductor materials, hydrogenated amorphous-Si (a-Si:H) has been studied for its advantage of high light collection efficiency,[9] but this material suffers from limitation due to long-lived traps.[10] Indium−gallium−arsenide (InGaAs) photodiodes showed a good potential for imaging in the near-infrared (NIR) region by integration on CMOS-based circuit.[11] Colloidal quantum-dot (CQD) or quantum-dot embedded in polymer processed in solution has received much attention to enhance the sensitivity.[6,12,13] Recently, a graphene-based photodetector with improved absorption as compared to its original low value has been reported with the advantages of ultrafast response and efficient photocarrier separation.[14] However, most inorganic semiconducting materials, due to their broad absorption spectra extending from the visible to the infrared (IR) region, are not eligible for the color-selective photodetection.

Conjugated organic small molecules or polymers with their easily tunable absorption in the visible spectrum are interesting candidates as image sensor application. It was demonstrated that a hybrid CMOS-imager using poly(3-hexylthiophene-2,5-diyl) (P3HT):[6,6]-phenyl C_{61} butyric acid methyl ester (PCBM) in a bulk-heterojunction (BHJ) structure as an active layer suppressed the optical and electrical crosstalk due to the high coefficient of absorption of the polymer and the low mobility in BHJ active layers, respectively.[15] However because of the broad EQE absorption spectrum between 400 nm and 650 nm, another color separation system for realization of color image should be added. For the practical reduction of spectral crosstalk, the use of organic semiconducting small molecules with specific absorption ranges for respective RGB subpixels is promising for the replacement of Si PD. Recently, organic small molecules with specific spectral photoresponse have been exploited for this purpose.[16,17]

Boron-subphthalocyanine chloride (SubPc) has been widely used for optoelectronic applications, particularly in organic photovoltaic device (OPV) owing to its high coefficient of absorption while its relatively large band gap led to the enhancement of open-circuit voltage (V_{OC}).[18−22] On the other hand, narrow absorption bandwidth of SubPc generates rather low short circuit current (J_{SC}), severely limiting the device performances.[22] As organic photodetector (OPD) application however, this character of SubPc can be better exploited for spectral sensitivity.

In this study, we demonstrate the highly green-sensitive OPD with a BHJ structure comprising SubPc and other materials, which showed potential for highly green-sensitive OPDs.[23] We investigated the electrical behavior and device efficiency of the OPD, from which the parameters of overall specific detectivity and spectral photoresponsivity were extracted. To interpret the spectral response of EQE spectra in detail, the photoresponsivities converted from EQEs are compared with the practical absorptions corrected by reflectances of the active BHJ layers. Finally, we calculated the spectral crosstalk based on the model used in a conventional image sensor pixel arrays, and investigated the relationship between the sensitivity and spectral selectivity.[8]

EXPERIMENTAL METHODS

The molecular structures of the materials used in this study are shown in Figure 1a. SubPc and *N*,*N*-dimethyl quinacridone (DMQA) were purchased from Lumtec Technology Corp., whereas pentafluoro-phenoxy substituted boron subphthalocyanine (F5-SubPc)[24] and dibutyl substituted dicyanovinyl terthiophene (DCV3T)[25] were synthesized according to the previous literature.

The organic photodiodes were fabricated on glass substrates precoated with indium−tin-oxide (ITO) with a sheet resistance of 15 Ω per square, as the anode. A 30 nm thick molybdenum oxide (MoO_x) layer was further deposited on the ITO. And then the organic BHJ layers with the thickness of 90 nm were deposited by vacuum thermal evaporation at a base pressure of $<2 \times 10^{-7}$ Torr, and the composition ratio between a donor and an acceptor was controlled as same ratios at the deposition rate of 0.1 nm/s. The Al cathode was finally evaporated at a rate of 0.2 nm/s through a shadow mask with an active area of 0.04 cm^2. Four OPD devices with different donor/acceptor materials combination were fabricated: device A (SubPc/F5-SubPc), device B (SubPc/DCV3T), device C (DMQA/SubPc), and device D (DMQA/F5-SubPc). After cathode deposition, glass encapsulation was immediately performed under nitrogen by using a UV curable resin as sealant. The device stability was monitored by measuring the current−voltage characteristics that did not change significantly over 6 months.

The optical spectra of absorbance, transmittance, and reflectance of the respective organic films grown on glass substrates were measured using a Shimadzu UV-2450 spectrophotometer. The ionization potential of organic thin film was measured by using a photoelectron spectrometer in air (AC-2, RKI Instrument Co. Ltd.).

The charge transport characteristics of the individual materials were investigated by measuring the single carrier mobilities. The hole-only devices were fabricated by depositing a 30 nm MoO_x film on the ITO-coated glass substrate, on top of which were deposited sequentially a 100 nm active layer, a 30 nm MoO_x layer, and an 80 nm Al electrode layer. The electron-only devices were prepared by the sequential deposition of a 100 nm active layer on the ITO, an ultrathin LiF layer and an Al cathode.

The external quantum efficiency (EQE) of OPD devices was measured using a spectral incident photon-to-current efficiency (IPCE) measurement system while illuminating monochromatic light generated by an ozone-free Xe lamp with a chopper frequency of 30 Hz. A calibrated Si-PD was used to measure the incident monochromatic light intensity. The current−voltage (J−V) curves were measured using a Keithley K4200 semiconductor parameter analyzer, and the light response was measured under illumination from a white LED with a broad range of emission wavelengths of 400−675 nm and light output intensity of approximately 1 mW/cm^2.

RESULTS AND DISCUSSION

Figure 1b shows the film absorption spectra in the visible region of the different materials taken separately. SubPc shows the prominent lowest energy absorption band between the wavelengths of 560−600 nm, known as the Q-band resulting from the $C3\nu$ symmetric ligand/molecular fragment.[26] The absorption spectra confirms high green color sensitivity of SubPc, with a maximum wavelength (λ_{max}) at 586 nm, a high absorption coefficient of approximately 1.4×10^5 cm^{-1}, and a narrow full-width-at-half-maximum (FWHM) of 80 nm. Despite the change in electronic character, from p- to n-type, the absorption spectra of F5-SubPc exhibit moderate variation as compared with those of SubPc, with a λ_{max} at 581 nm, a high absorption coefficient of 1.47×10^5 cm^{-1}, and narrower FWHM of 49 nm. It was previously reported that axial substitutions on SubPc have little effect on the shift of absorption band position.[27] DMQA shows low absorption with narrow FWHM, whereas DCV3T shows high absorption but relatively wide FWHM.[28,29]

The potential of SubPc as a donor was first examined in combination with DCV3T and F5-SubPc as acceptors in devices A and B, respectively. Then, the possibility of using either SubPc or its derivative F5-SubPc as acceptor was evaluated by choosing DMQA as the donor, in device C and D, respectively. For the choice of donor and acceptor, it is necessary to consider the offset of LUMO levels between the two respective active materials. Except for composition A with an offset of 0.2 eV, all LUMO level differences for the other device compositions were above 0.4 eV, which is sufficient for efficient charge separation.[30] Despite its small offset, device A has a potential for high EQE and good rectification, as shown in a previous study[26] in the field of OPV, where this composition was used to build planar heterojunction structures. In Figure 1d, the absorbance spectra of all four BHJ films are consistent with the absorption coefficient spectra of the single active materials shown in Figure 1b. Regarding the basic transport properties of these active materials, the charge mobilities measured by space-charge-limited-current (SCLC) model[31] are shown in the Table S1 in the Supporting Information. The hole mobilities were similar for DMQA and SubPc with values of 1.62×10^{-8} and 8.95×10^{-8} $cm^2/(V\ s)$ at an applied electric field of 0.3 MV/cm, respectively, whereas the electron mobilities were different by orders of magnitude with values of 2.73×10^{-8} for DCV3T, 1.36×10^{-9} for SubPc, and 1.93×10^{-10} $cm^2/(V\ s)$ for F5-SubPc. The difference in h+/e− mobilities for SubPc is consistent with the values reported in a previous study.[21] For the unambiguous characterization of the device performance, the structure of the OPDs was fabricated to be rather simple by avoiding the use of additional interlayers that could further complicate the analysis by introducing new interfaces in the system.

As the basic performances of the photodetectors, the current density−voltage (J−V) characteristics and the EQE spectra of devices A−D are shown in Figure 2. The fundamental parameters of OPD devices are extracted from Figure 2 and summarized in Table 1. All devices exhibited similar levels of reverse dark current densities (J_d), within the same order of magnitude, from 4×10^{-8} to 9×10^{-8} A/cm^2 at an applied voltage of −5 V. This particularly low J_d, considering the

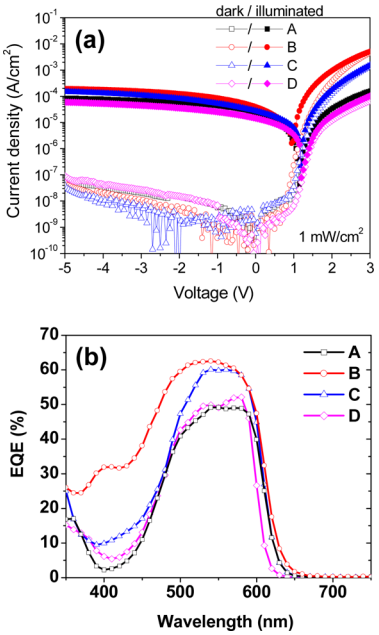

Figure 2. (a) Current density−voltage characteristics in the dark and under illumination at 1 mW/cm^2 for the four OPDs and (b) external quantum efficiency (EQE) spectra at an applied voltage of −5 V. Device descriptions are as follows: (A) SubPc/F5-SubPc, (B) SubPc/DCV3T, (C) DMQA/SubPc, and (D) DMQA/F5-SubPc as donors and acceptor.

Table 1. Electrical Parameters of the Four OPD Devices Decomposed in Terms of Detectivity, Sensitivity, and Spectral Selectivity at the Applied Voltage of −5 V[a]

	detectivity		sensitivity		selectivity	
device	J_d (A/cm^2)	D^* @550 nm (cm Hz$^{1/2}$/W)	λ_{max} (nm)	EQE @λ_{max} (%)	EQE @450 nm (%)	FWHM (nm)
A	6.79×10^{-8}	1.48×10^{12}	550	49.2	11.0	137
B	5.31×10^{-8}	2.12×10^{12}	540	62.6	38.1	211
C	4.01×10^{-8}	2.34×10^{12}	560	60.1	17.1	131
D	8.99×10^{-8}	1.28×10^{12}	580	52.2	13.1	126

[a]Abbreviations: dark current density (J_d), specific detectivity (D^*), external quantum efficiency (EQE), and full-width-at-half-maximum (FWHM).

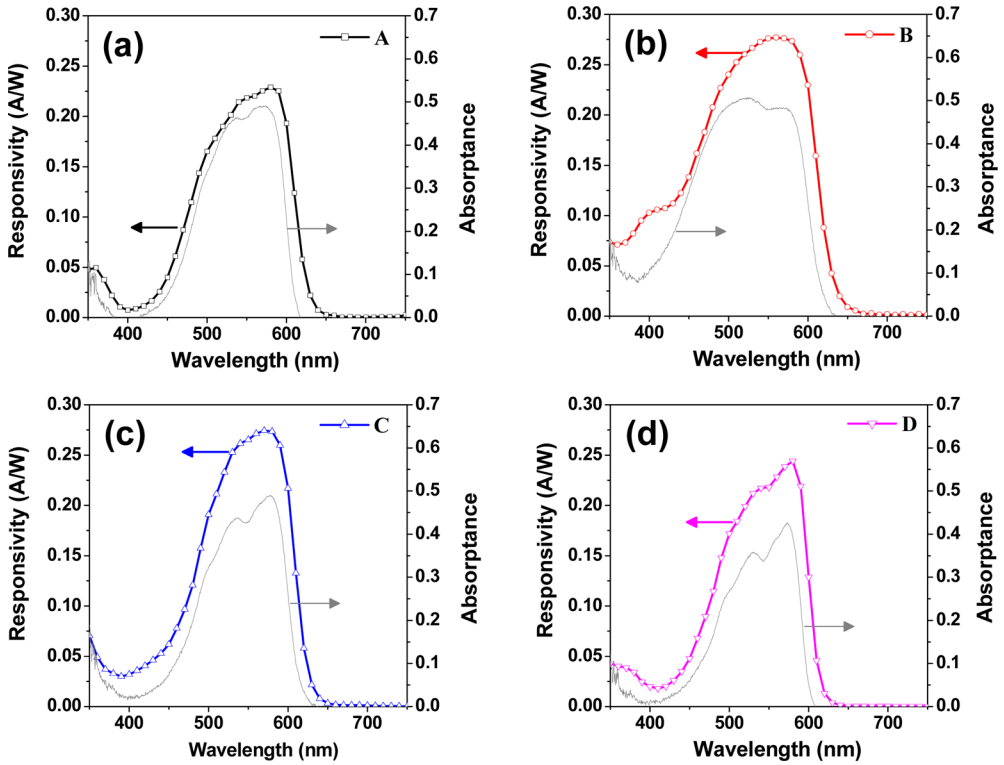

Figure 3. Comparison between the photoresponsivity spectra of the OPD devices at an applied voltage of −5 V and absorptance spectra of the four active BHJ films. The device descriptions are as follows: (a) A with SubPc/F5-SubPc, (b) B with SubPc/DCV3T, (c) C with DMQA/SubPc, and (d) D with DMQA/F5-SubPc as donors and acceptors.

absence of any electron or hole blocking layers in the simple device structure, reflects the absence of leakage current. Under illumination at a light intensity of 1 mW/cm^2, the photogenerated current densities (J_{ph}) of all four devices significantly increased by two orders of magnitude. However the ratio J_{ph}/J_d was different depending on the devices. Devices B and C exhibit relatively high J_{ph}/J_d ratios of 3.99×10^3 and 3.69×10^3, respectively, while devices A and D show relatively low J_{ph}/J_d ratios of 1.26×10^3 and 6.64×10^2 at the applied voltage of −5 V, respectively. From the results of devices B and C, it appears that SubPc can work as a donor or an acceptor, as long as energy levels are matched.[20] Additionally, the orders in J_{ph}/J_d ratios are consistent with the orders of forward photocurrent densities, which are 5.00×10^{-3} A/cm^2 for B, 1.52×10^{-3} A/cm^2 for C, 1.61×10^{-4} A/cm^2 for A, and 1.02×10^{-4} A/cm^2 for D at the applied voltage of 3 V. It has been reported that the forward current reduction under illumination influences the charge transport in devices composed of the same materials, resulting in variation in device efficiency.[31,32]

In addition, we evaluated the specific detectivity as the green-sensitivity parameter considering dark current noise, related with device efficiency, as shown in Table 1. The specific detectivity (D^*) can be calculated from the expression of $D^* = (J_{ph}/L_{light})/(2qJ_d)^{0.5}$, where J_{ph} is the photocurrent density at the incident light intensity (L_{light}) at the wavelength of 550 nm and q is the absolute value of electron charge (1.6×10^{-19} C). Device C shows the highest value of 2.34×10^{12} cm·Hz$^{0.5}$/W owing to the high photocurrent and low dark-current. The high D^* values over 10^{12} cm·Hz$^{0.5}$/W of all devices are comparable with the detectivity of photodetectors based on polymers or inorganic materials.[33,34]

To evaluate the spectral selectivity at the respective wavelength, the EQE plots of the four OPDs at the applied voltage of −5 V were measured, as shown in Figure 2b. In the target wavelength range of green color, between 500 and 600 nm, devices B and C exhibited high EQE values of 62.6% at 540 nm and 60.1% at 560 nm, respectively, while the devices D and A showed relatively low values of 52.2 % at 580 nm and 49.2 % at 550 nm, respectively. Despite the EQE being a function of different interdependent factors, it is noted here that these EQE values correlate with the electron mobilities of individual materials taken as acceptors. It would imply that electron

mobility, lower than the hole mobility, is the transport limiting factor. Meanwhile, the EQEs also show nontrivial intensity in the blue-color region between 400 and 500 nm, which may aggravate the spectral crosstalk. At the wavelength of 450 nm, device B showed the highest value of 38.1% due to the broad absorption of DCV3T used as an acceptor, but the other devices also exhibited over 10% EQEs despite the quite low absorption in the blue region of DMQA and SubPc derivatives. The exact EQE and λ_{max} values extracted from Figure 2b are presented in Table 1. The FWHMs used as the simple index for the spectral selectivity[35] exhibited the highest value of 211 nm for device B with the best EQE, and secondly 137 nm for device A due to the low EQE value despite narrow absorption bandwidths of both donor and acceptor materials. It is noted that there is a conflict between high EQE and narrow FWHM. In the EQE spectra of Figure 2b, it is interesting to note that λ_{max} at 550 nm is significantly shifted as compared to the highest absorption of SubPc derivatives at 580 nm, as shown in Figure 1d. This is beneficial for the spectral sensitivity of a green-sensitive OPD.

To understand the difference between the EQE spectra of the OPD devices and the absorption spectra of the materials, we analyzed the optical properties of the four BHJ films including the transmittance, reflectance, and absorbance that can be simply measured by UV−vis spectroscopy. The term of absorbance is defined as the logarithmic ratio between the radiation falling upon a material and the radiation transmitted through a material, which is used as a conventional optical parameter of photopigment. In contrast, the absorptance is the absorption fraction out of the whole incident radiation flux, which complements the fractions of transmission and reflection.[36] Absorptance is thus the reflection-corrected absorption characteristic, which can be estimated by subtracting transmittance and reflectance from optical unity. The transmittance and reflectance spectra of four BHJ films are shown in Figure S1 (Supporting Information).

In Figure 3, all absorptance spectra exhibit blunt shapes with a reduction of maximum absorption (see Figure 1d), which is induced from the reflectance effect. Whereas SubPc has proper property in terms of absorption, at 586 nm, the films comprising SubPc show high reflectance at the wavelength of 605 nm (Figure S1b). Device D without SubPc showed the maximum reflectance at the wavelength of 594 nm (Figure S1b), resulting in the same behavior but different peak position compared with other devices including SubPc, which implies that the high reflectance at 605 nm is caused by SubPc. With these practical absorption properties of BHJ layers corrected by reflections, we compared the photoresponsivity (as the spectral sensitivity) for the OPD devices in Figure 3. The photoresponsivity (R) is defined as $R[A/W] = J_{ph}/L_{light} = EQE/h\nu$, where $h\nu$ is the energy of the incident photon in electron volts (eV).[33,37] For devices A, C, and D, the R profiles are consistent with the absorptance profiles, as the maximum peak intensities are located at the same wavelength. In contrast, device B composed of SubPc and DCV3T shows a broader spectral responsivity with λ_{max} at 560 nm, which reflects that the absorptance is dominated by the absorption of DCV3T. The valley present around 540 nm in the absorptance spectrum is not visible in the photoresponsivity spectrum because of the applied bias voltage of −5 V. The R values could be simply converted to the EQE spectra, as shown in Figure 2b, after correction with the photon energy of the respective wavelength. Whereas the R values are similar in the blue and red regions, the EQE spectra show an amplified shoulder in the blue region compared to that in the red region due to the difference in photon energy.

In conventional image sensor arrays with color pixels, the spectral crosstalk usually corresponds to the ratio between the target signal (i.e. a signal in a green-absorbing pixel under green light illumination) and the undesirable signal (a signal in a green-absorbing pixel under blue- or red-light illumination). The signal is defined by the integral of photoresponsivity as spectral response at the specific wavelength region.[8] Although the single color unit OPD is investigated in this study, the guide line for color selectivity is needed. Hence, we examined the modified spectral crosstalk, which is defined as the ratio between the signal in green-region and the signal in blue- or red-region within a single responsivity spectrum. The specific wavelength regions are divided in blue (440−500 nm), green (510−570 nm), and red (590−650 nm) region according to conventional image sensor. Figure 4a shows the spectral

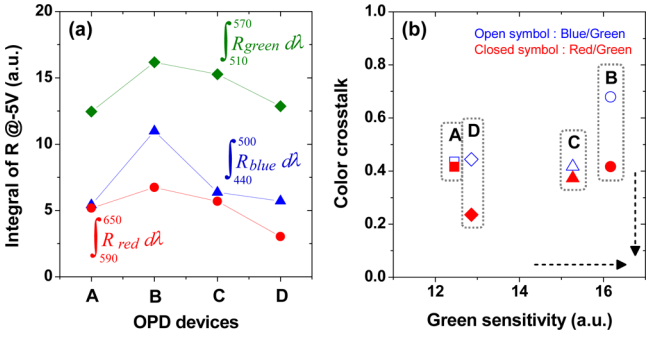

Figure 4. (a) Spectral responses from the integral of responsivity within specific wavelength regions. (b) Green-sensitivity and spectral crosstalk of the four OPD devices.

responses by integrating the photoresponsivity within the specific wavelength regions. Among the four devices, device B exhibits the highest integrated R value in the green region, however, with also pronounced R values in the blue and red regions. In contrast, device D showed a particularly low spectral response in the red region as well as in the green region. In Figure 4b, the green-sensitivity-spectral crosstalk characteristics are represented by using the integral of R values in the green region and the ratio of integral values at blue/green regions and red/green regions. In terms of selectivity, device D showed the lowest red crosstalk around 0.2, as the consequence of the presence of F5-SubPc, which induced an enhanced blue-shifted absorption in the blend film, as compared with SubPc. However, the green-sensitivity of devices A and D is especially low. The sensitivity of device C is improved by around 17% in comparison with device D, as a result of the difference of maximum EQE values. In contrast, device B shows the highest green-sensitivity with the desirable maximum peak position, even though the blue sensitivity exhibits a factor of 0.7 of the green-sensitivity. From a comprehensive perspective, device C exhibits optimized performance in terms of high spectral sensitivity and selectivity.

To this point, on the basis of material properties and device characterization, it appears that it is difficult to achieve simultaneously high green-sensitive OPD with low blue crosstalk. High EQEs in the green-region have been reported in numerous devices, which however needed an additional color filter for specific color recognition due to their wide

bandwidth.[9−14] On the contrary, a device with narrow FWHM under 100 nm has been reported with an efficiency under 1% at the applied voltage of −1.5 V.[38] It was reported that the blend layer thickness can be used to control the spectral selectivity, but may lead to limited sensitivity at high bias due to the absorption limitation of materials.[37] In this study, it is shown that SubPc derivatives are attractive material candidates for green-sensitive OPD with the merit of high absorption coefficient in the green region and narrow FWHM. Additionally, the control of charge generation through proper energy levels and balanced charge transport is a prerequisite to achieve high sensitivity.[23] Considering these different aspects, it comes out that device C composed of DMQA and SubPc, characterized by reduced blue crosstalk with sufficient green-sensitivity, presents the ideal material combination for OPD application.

CONCLUSIONS

We have investigated the green-sensitive OPD with high spectral sensitivity and selectivity using SubPc derivatives for organic image sensor applications. The optimized composition is achieved by blending DMQA as the donor and SubPc as the acceptor, and the performances exhibit high D^* of 2.34×10^{12} cm $Hz^{0.5}$/W, EQE value of 60.1% at −5 V, and small FWHM of 131 nm. In spite of the sharp absorption property of SubPc with λ_{max} at 586 nm, the EQE spectrum showed favorable green-sensitivity characterized by smooth waveform with λ_{max} at 560 nm, which is induced from the high reflectance with λ_{max} at 605 nm. The highly green-sensitive OPD with low blue crosstalk is difficult to achieve; nevertheless, the device comprising DMQA and SubPc realized the reduced blue-crosstalk and the high green-sensitivity, demonstrating its promising potential for application to CMOS image sensors.

ASSOCIATED CONTENT

Supporting Information

Carrier mobilities of the individual materials by SCLC method and optical properties of transmittance and reflectance of the four BHJ films on the glass substrate. This material is available free of charge via the Internet at http://pubs.acs.org.

AUTHOR INFORMATION

Corresponding Authors

*E-mail: ywjin@samsung.com (Y.W.J.).
*E-mail: parksy@snu.ac.kr (S.Y.P.).

Notes

The authors declare no competing financial interest.

ACKNOWLEDGMENTS

This work was supported by the National Research Foundation of Korea (NRF) grant funded by the Korea government (MSIP) (No. 2009-0081571).

REFERENCES

(1) Martino, N.; Ghezzi, D.; Benfenati, F.; Lanzani, G.; Antognazza, M. R. *J. Mater. Chem. B* **2013**, *1*, 3768−3780.
(2) Xu, X.; Davanco, M.; Qi, X.; Forrest, S. R. *Org. Electron.* **2008**, *9*, 1122−1127.
(3) Someya, T.; Kato, Y.; Iba, S.; Noguchi, Y.; Sekitani, T.; Kawaguchi, H.; Sakurai, T. *IEEE Trans. Electron Devices* **2005**, *52*, 2502−2511.
(4) El Gamal, A.; Eltoukhy, H. *IEEE Circuits Devices Mag.* **2005**, *21*, 6−20.
(5) El-Desouki, M.; Deen, M. J.; Fang, Q.; Liu, L.; Tse, F.; Armstrong, D. *Sensors* **2009**, *9*, 430−444.
(6) Konstantatos, G.; Clifford, J.; Levina, L.; Sargent, E. H. *Nat. Photonics* **2007**, *1*, 531−534.
(7) Ihama, M.; Mitsui, T.; Nomura, K.; Maehara, Y.; Inomata, H.; Gotou, T.; Takeuchi, Y. *IDW 09, Proc. 16th Int. Display Workshops* **2009**, INP1−4.
(8) Agranov, G.; Berezin, V.; Tsai, R. H. *IEEE Trans. Electron Devices* **2003**, *50*, 4−11.
(9) Theil, J. A.; Snyder, R.; Hula, D.; Lindahl, K.; Haddad, H.; Roland, J. *J. Non-Cryst. Solids* **2002**, *299-302*, 1234−1239.
(10) Vygranenko, Y.; Chang, J. H.; Nathan, A. *IEEE J. Quantum Electron.* **2005**, *41*, 697−703.
(11) Barton, J. B.; Cannata, R. F.; Petronio, S. M. *Proc. SPIE* **2002**, *4721*, 37−47.
(12) Konstantatos, G.; Sargent, E. H. *Nat. Nanotechnol.* **2010**, *5*, 391−400.
(13) Rauch, T.; Boberl, M.; Tedde, S. F.; Furst, J.; Kovalenko, M. V.; Hesser, G.; Lemmer, U.; Heiss, W.; Hayden, O. *Nat. Photonics* **2009**, *3*, 332−336.
(14) Gan, X.; Shiue, R.-J.; Gao, Y.; Meric, I.; Heinz, T. F.; Shepard, K.; Hone, J.; Assefa, S.; Englund, D. *Nat. Photonics* **2013**, *7*, 883−887.
(15) Baierl, D.; Pancheri, L.; Schmidt, M.; Stoppa, D.; Betta, G.-F. D.; Scarpa, G.; Lugli, P. *Nat. Commun.* **2012**, *3*, 1175.
(16) Lin, Y.; Lia, Y.; Zhan, X. *Chem. Soc. Rev.* **2012**, *41*, 4245−4272.
(17) Baeg, K.-J.; Binda, M.; Natali, D.; Caironi, M.; Noh, Y.-Y. *Adv. Mater.* **2013**, *25*, 4267−4295.
(18) Gommans, H.; Cheyns, D.; Aernouts, T.; Girotto, C.; Poortmans, J.; Heremans, P. *Adv. Funct. Mater.* **2007**, *17*, 2653−2658.
(19) Gommans, H.; Aernouts, T.; Verreet, B.; Heremans, P.; Medina, A.; Claessens, C. G.; Torres, T. *Adv. Funct. Mater.* **2009**, *19*, 3435−3439.
(20) Beaumont, N.; Cho, S. W.; Sullivan, P.; Newby, D.; Smith, K. E.; Jones, T. S. *Adv. Funct. Mater.* **2012**, *22*, 561−566.
(21) Pandey, R.; Gunawan, A. A.; Mkhoyan, K. A.; Holmes, R. J. *Adv. Funct. Mater.* **2012**, *22*, 617−624.
(22) Sullivan, P.; Duraud, A.; Hancox, I.; Beaumont, N.; Mirri, G.; Tucker, J. H. R.; Hatton, R. A.; Shipman, M.; Jones, T. S. *Adv. Funct. Mater.* **2011**, *21*, 352−355.
(23) Lee, K.-H.; Leem, D.-S.; Sul, S.; Park, K.-B.; Lim, S.-J.; Han, H.; Kim, K.-S.; Jin, Y. W.; Lee, S.; Park, S. Y. *J. Mater. Chem. C* **2013**, *1*, 2666−2671.
(24) Morse, G. E.; Helander, M. G.; Maka, J. F.; Lu, Z.-H.; Bender, T. P. *ACS Appl. Mater. Interfaces* **2010**, *2*, 1934−1944.
(25) Uhrich, C.; Schueppel, R.; Petrich, A.; Pfeiffer, M.; Leo, K.; Brier, E.; Kilickiran, P.; Baeuerle, P. *Adv. Funct. Mater.* **2007**, *17*, 2991−2999.
(26) Morse, E.; Bender, T. P. *ACS Appl. Mater. Interfaces* **2012**, *4*, 5055−5068.
(27) Claessens, C. G.; González-Rodríguez, D.; Torres, T. *Chem. Rev.* **2012**, *102*, 835−853.
(28) Mizuguchi, J.; Senju, T. *J. Phys. Chem. B* **2006**, *110*, 19154−19161.
(29) Ziehlke, H.; Fitzner, R.; Koerner, C.; Gresser, R.; Reinold, E.; Bäuerle, P.; Leo, K.; Riede, M. K. *J. Phys. Chem. A* **2011**, *115*, 8437−8446.
(30) Dennler, G.; Scharber, M. C.; Brabec, C. *Adv. Mater.* **2009**, *21*, 1323−1338.
(31) Mihailetchi, V. D.; Xie, H. X.; de Boer, B.; Koster, L. J. A.; Blom, P. W. M. *Adv. Funct. Mater.* **2006**, *16*, 699−708.
(32) Lenes, M.; Morana, M.; Brabec, C. J.; Blom, P. W. M. *Adv. Funct. Mater.* **2009**, *19*, 1106−1111.
(33) Gong, X.; Tong, M.; Xia, Y.; Cai, W.; Moon, J. S.; Cao, Y.; Yu, G.; Shieh, C.-L.; Nilsson, B.; Heeger, A. J. *Science* **2009**, *325*, 1665−1667.
(34) Tedde, S. F.; Kern, J.; Sterzl, T.; Fürst, J.; Lugli, P.; Hayden, O. *Nano Lett.* **2009**, *9*, 980−983.
(35) Vuuren, R. D. J.; Pivrikas, A.; Pandey, A. K.; Burn, P. L. *J. Mater. Chem. C* **2013**, *1*, 3532−3543.

(36) Bass, M.; Van Stryland, E. W.; Williams, D. R.; Wolfe, W. L. In *Handbook of Optics*; McGraw-Hill: New York, 1995; Chap. 25.
(37) Leem, D.-S.; Lee, K.-H.; Park, K.-B.; Lim, S.-J.; Kim, K.-S.; Jin, Y. W.; Lee, S. *Appl. Phys. Lett.* **2013**, *103*, 043305.
(38) Fukuda, T.; Komoriya, M.; Kobayashi, R.; Ishimaru, Y.; Kamata, N. *Jpn. J. Appl. Phys.* **2009**, *48*, 04C162.